Single ether-based side chains in conjugated polymers: Towards power factors of 2.9 mW/m . K 2

Pablo Durand, Huiyan Zeng, Till Biskup, Vishnu Vijayakumar, Viktoriia Untilova, Céline Kiefer, Benoît Heinrich, Laurent Herrmann, Martin Brinkmann, Nicolas Leclerc

Single ether-based side chains in conjugated polymers: Towards power factors of 2.9 mW/m·K^2.

Pablo Durand[1], Huiyan Zeng[2], Till Biskup[3], Vishnu Vijayakumar[2], Viktoriia Untilova[2], Céline Kiefer[4], Benoît Heinrich[4], Laurent Herrmann[2], Martin Brinkmann[2*], Nicolas Leclerc[1*]

(1) Université de Strasbourg, CNRS, ICPEES UMR 7515, F-67087 Strasbourg, France

(2) Université de Strasbourg, CNRS, ICS UPR 22, F-67000 Strasbourg, France

(3) Universität des Saarlandes, Physikalische Chemie, Campus B2 2, 66123 Saarbrücken, Germany

(4) Université de Strasbourg, CNRS, IPCMS UMR 7504, F-67034 Strasbourg, France

Corresponding authors:

Nicolas Leclerc: leclercn@unistra.fr

Martin Brinkmann: martin.brinkmann@ics-cnrs.unistra.fr

Abstract

Combining side chain engineering and controlled alignment of PBTTT is an effective strategy to produce oriented thin films with improved thermoelectric performances when doped sequentially with the acceptor molecule F_6TCNNQ. The substitution of linear alkyl side-chains (*n*-C_{12}) with a chain of identical length including an ether function (*n*-C_7OC_4) leads to a new class of slightly polar PBTTT polymers, preserving the ease of synthesis and air stability of alkylated PBTTTs. This side-chain modification improves the structural order of PBTTT backbones and the thermomechanical

properties of the polymer. It then can be oriented by high temperature rubbing up to 240°C to reach very high dichroic ratios up to 20 thanks to enhanced cohesive forces within side-chain layers. The side chain polarity of *n*-C_7OC_4 helps to tune the polymer-dopant interactions. A multi-technique approach demonstrates that F_6TCNNQ dopants are randomly oriented in the disordered side chain layers of *n*-C_7OC_4 with some evidence of dopant clustering. The combination of improved alignment and random orientation of intercalated F_6TCNNQ dopants helps reach a very high charge conductivity $\sigma = 5 \cdot 10^4$ S/cm and a record power factors PF = 2.9 $mWm^{-1}K^{-2}$ in the polymer chain direction.

1. Introduction

Conjugated polymers are central materials in organic electronics as they combine numerous advantages related to flexibility, ease of processing and relatively low cost that were used with remarkable success for the production of displays and photovoltaic devices.[1,2] The advances and breakthroughs in the synthesis of polymer semiconductors (PSCs) have recently been used in the emerging field of organic thermoelectric (TE) materials.[3,4] TE materials have the unique ability to transform heat into electricity but their performances are determined by the dimensionless parameter $ZT=\sigma S^2/\kappa$ that depends on essential parameters such as the charge conductivity σ, the Seebeck coefficient S and the thermal conductivity κ.[5] Ideally, a good TE material should exhibit high σ and S and low κ. One of the most popular approach to produce TE polymers consists in doping PSCs using dopant molecules with suitable energy levels (i.e. high electron affinity (EA) for *p*-type doping and low ionization potential (IP) for *n*-type doping, respectively) to carry out redox processes with the PSC.[6] The doping efficiency and consequently the ultimate charge conductivity depend on various material parameters such as the offset between the frontier molecular orbital energy levels of the dopants and PSCs,[7] the solid-state order of doped PSCs,[8] as well as the dopant location with respect to the PSC backbone.[9,10] In this respect, side chain engineering is a well-established and powerful approach to tune the solid-state structure and consequently the charge

transport properties of PSCs.[11] It has been successfully used in TE by the introduction of polar oligoethylene glycol (OEG) side-chains. Such side chains influence the PSC's properties in different ways: i) they modify the PSCs solubility in organic solvents enabling their swelling in polar media,[12] ii) they can lead to a decrease of the π-π stacking distance[13] and iii) they help increase significantly the dopant-polymer miscibility/compatibility[14] and stability.[15] As an example, PEGylated thiophene-based polymers can be solubilized in a polar solvent along with the dopant tetrafluoro-tetracyanoquinodimethane (F_4TCNQ) without precipitation of the doped system.[16] The coprocessing of the polymer with the dopant helped to reach higher doping levels as well as a better thermal stability of the dopant/polymer pair.[17] In addition, the alkoxy nature of the short OEG side chains helped reduce significantly the IP of the conjugated polymer, making it possible to reach double doping of the polymer p($g_4$2T-TT) with acceptor molecules such as F_4TCNQ or hexafluoro-tetracyanonaphthoquinodimethane (F_6TCNNQ).[7,18] Although the conductivities and Seebeck coefficients are significantly lower than the values obtained for *p*-type materials, similar positive effects of PEGylation have been demonstrated for *n*-type polymers.[14,19] On the down side, the OEG side chains, are highly hygroscopic and can lead to a reduced thermal stability of the resulting polymers.[18,20] Moreover, the electron donating effect of alkoxy side chains leads to highly light and air sensitive monomers and polymers (i.e. the air stability threshold is considered to be around $E_{HOMO} \approx$ -5.2 eV) and it is consequently necessary to properly protect the reaction intermediates and final materials against oxidation.[21,22] From a synthesis point of view, the high polarity and lower crystallinity of the reaction intermediates make the purification of PEGylated polymers particularly complex and cumbersome.[23] In addition, if the improvement of polymer solubility in polar media is an appealing feature for coprocessing, it turns out to be a weakness for the best performing sequential doping approach, which consists in doping a material already processed with an orthogonal solvent.[24] From a structural point of view, Thelakkat *et al.* demonstrated that grafting OEG side chains directly on the conjugated backbone significantly decreases the polymer structural order as well as the charge mobility.[25] The adverse effect of

incorporating OEG side chains on the charge conductivity of a series of F_4TCNQ-doped polythiophenes was also recently demonstrated by Nielsen *et al.*[26] The reduced charge conductivity could be ascribed to the detrimental effect of statistical OEG side chain incorporation on the solid state packing of the poly(thiophene)s.

Several recent studies highlighted the key role of structural order on the conductivity and TE properties of OSCs.[27] Growing highly ordered PSC-dopant systems is possible by playing with the crystallinity of the PSC prior to doping and by optimizing the method of dopant introduction inside the polymer matrix.[27,28-30] Moreover, polymer orientation was shown to lead to a concomitant increase of both charge conductivity σ and Seebeck coefficient S along the chain direction, demonstrating a simple means to enhance the thermoelectric power factor (PF) of doped PSCs. In the case of PBTTT-C_{12} doped with $FeCl_3$, record charge conductivities of 10^5 S/cm similar to those obtained for iodine-doped polyacetylene were obtained with power factors of 2000 $\mu W/mK^2$.[31] In particular, the ordering of dopant molecules inside the crystalline domains of P3HT or PBTTT was shown to determine to a certain extent the highest TE properties that can be reached. The packing and the length of side chains, the doping method (sequential doping, vapor phase doping) or the dopant geometry were found to be equally important to reach high TE PFs.[8,27,28,31]

Herein, in order to bring together the best of two worlds, we combine side chain engineering and controlled orientation/crystallization of PSCs to reach improved TE performances in oriented thin films of PBTTTs doped with F_6TCNNQ. Instead of using OEG side chains, we report the use of a single ether group within an alkyl side-chain. By substituting the C_{12} side-chain in PBTTT-C_{12} with a *n*-C_7OC_4 side-chain in the new PBTTT-^{8}O, a new class of slightly polar PBTTT-based PSCs is obtained, that preserves the ease of synthesis and air stability of alkylated PBTTTs. By carefully increasing the side chain polarity, we enhanced the polymer dopant interaction without damaging the well-known high structural order of PBTTT backbones. Also, such a minimal modification, while keeping solubility parameters comparable, extend the rubbing process temperature towards the polymer melting temperature, resulting in an improved polymer chains alignment. A

combination of differential scanning calorimetry (DSC), small and wide-angle X-ray scattering (SWAXS), polarized UV-vis-NIR absorption spectroscopy, Electron Paramagnetic Resonance (EPR) and Transmission Electron Microscopy (TEM) shows that the absence of crystallization and ordering of the side chains results in a random orientation of F_6TCNNQ dopants inside the side chain layers of the polymer with some evidence of clustering of dopant molecules. In strong contrast to PBTTT-C_{12}, thin films of PBTTT-^{8}O oriented by rubbing at 170°C show superior in-plane orientation (order parameters) and preservation of the pristine polymer structure when doped with F_6TCNNQ that lead to very high conductivity $\sigma = 5 \cdot 10^4$ S/cm and record power factors PF = 2.9 $mWm^{-1}K^{-2}$ in the chain direction. Moreover, it is worth to mention that, while such values are comparable to our previous record using the stronger oxidant $FeCl_3$, the TE performances stability of this F_6TCNNQ-doped PBTTT-^{8}O new system is also greatly improved.

2. Results and discussion

2.1. Polymer synthesis and characterizations

In order to investigate the effect of introducing a single ether group within the polymer side chains, we decided to keep the same chain length as our reference PBTTT-C_{12} polymer, namely a linear dodecyl chain. We simply substituted the 8th methylene group by an oxygen atom (see Figure 1a). Although it is not uncommon to find an ether function at the very beginning (alkoxy group) or end (methoxy group) of side chains, conjugated polymers including a single ether group somewhere else along their side chains are unusual.[32] In order to synthesize the new PBTTT-^{8}O, we investigated two different chemical pathways. The first one was a copy-paste of the standard PBTTT chemical route, using the corresponding brominated ether chain instead of the classical *n*-alkylbromide.[33] The issue came from the lack of total regioselectivity control that occur during the thiophene deprotonation/homocoupling sequence that lead to bithiophene regioisomers (namely head-to-tail and head-to-head byproducts). Such byproducts have similar polarity and are classically eliminated by recrystallization. Unfortunately, because of the ether side chain, these bithiophenes remains

liquid at room temperature preventing the use of recrystallization as purification technique. Considering that the ether function was responsible for this lack of crystallinity, we thus envisaged a second chemical route, which consisted in synthesizing the ether in the last step (see Scheme S1 in the Supporting Information). By keeping a terminal hydroxy group up to the bithiophene formation, we were able to recrystallize the resulting 5,5'-dibromo-4,4'-bis(7-hydroxyheptyl)-2,2'-bithiophene (compound **4** in scheme S1). Therefore, it has been synthesized in high yield and thoroughly purified to give the expected head-to-head regioisomer. A final step, which consisted in a Williamson reaction using KH as base and crown ether as catalyst yielded, after simple flash chromatography and almost quantitatively, a very pure 5,5'-dibromo-4,4'-bis(7-butoxyheptyl)-2,2'-bithiophene (compound **5** in scheme S1).

The two polymers, the standard alkyl-based side-chain and the new ether-based side-chain, were synthesized by Stille cross-coupling in identical conditions. They were characterized by size exclusion chromatography (SEC) in 1,2,4-TCB at 150°C and NMR (Figure S14 in the Supporting Information and Table 1). It is worth noting that both polymers show similar molar masses, around 30 kDa, allowing a proper comparison. In contrast to polymers presenting OEG polar side-chains, TGA analysis showed that stability was preserved by the introduction of a single ether group with a degradation temperature above 370°C (Figure S15). Cyclic voltammetry (CV) on thin films has been performed to estimate the highest occupied molecular orbital (HOMO) energy levels (Figure S16). It is worth mentioning that the new PBTTT-^{8}O exhibits a slightly lower oxidation potential than its PBTTT-C_{12} counterpart (-4.95eV and -5.10eV, respectively). As the two PSCs have identical conjugated backbones, we attributed this shift to the difference in ion penetration into the bulk during electrochemical redox reactions. Indeed, as already reported in literature, the slightly increased polarity of PBTTT-^{8}O is probably responsible for a small swelling in acetonitrile, leading to a faster diffusion of ions into the thin film volume.[12] This is confirmed by PESA measurements which give the same HOMO values, of -4.8 eV, for both polymers (Figures S17-S18). This PESA measurements highlight the lack of significant impact of ether group on intrinsic energy levels of

polymers. Accordingly, both polymers can be easily doped with F_6TCNNQ. Optical absorption properties have been studied in solution and thin-film (Figures S19 and S20). Solution spectra are almost identical for both polymers. However, despite the two polymers exhibit identical optical bandgap of about 1.9 eV, they show little differences in solid-state, indeed PBTTT-C_{12} exhibit a slightly more pronounced vibronic structure at low energy than PBTTT-^{8}O.

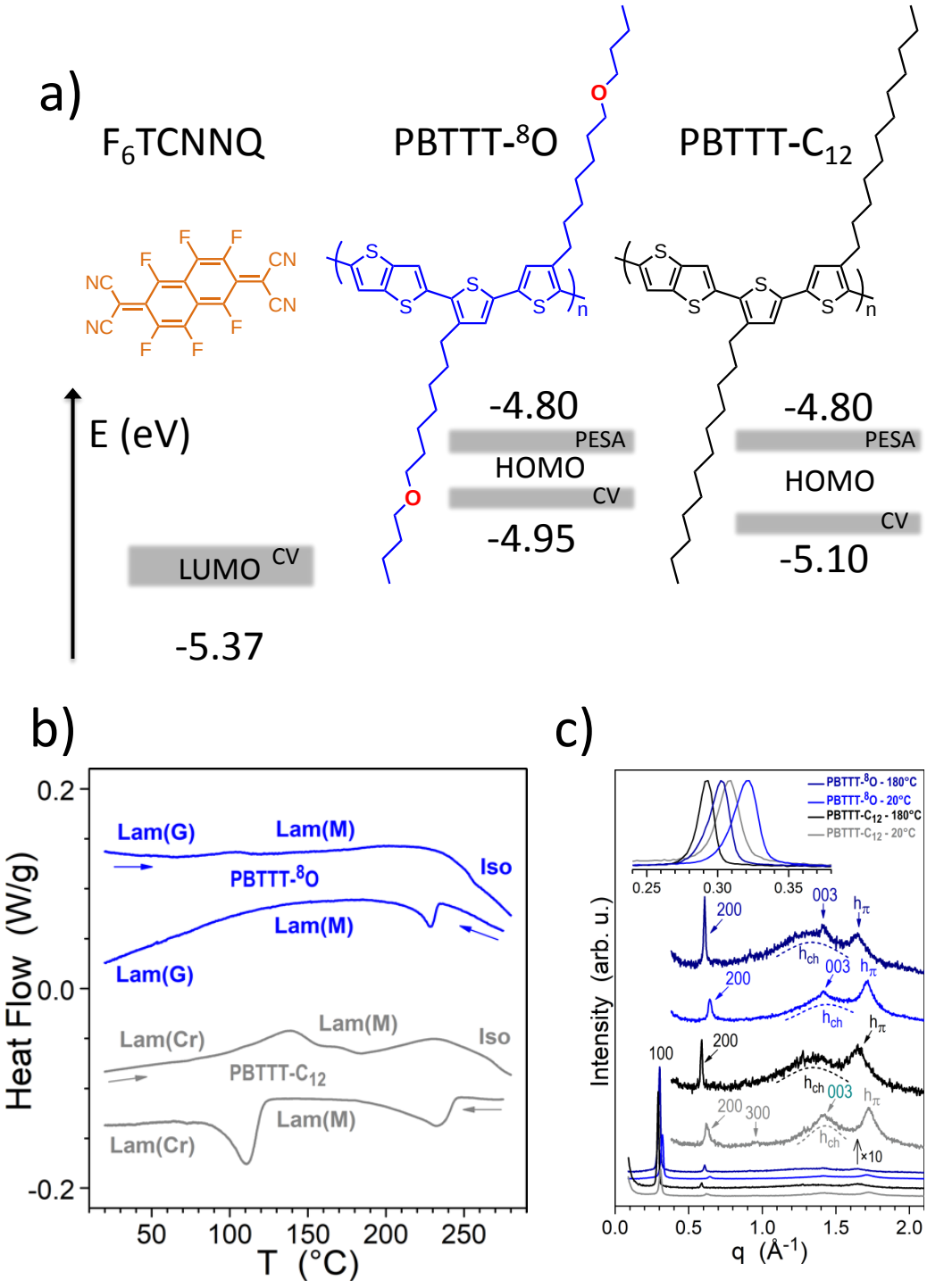

Figure 1. a) Chemical structures of the studied compounds and illustration of the energy level

positions of the PBTTTs HOMO (CV: measured by Cyclic Voltammetry; PESA: measured by PESA) and of the F_6TCNNQ Lowest Unoccupied Molecular Level (LUMO). b) DSC curves of the polymers on second heating and on cooling to RT (PBTTT-^{8}O in blue and PBTTT-C_{12} in black). b) SWAXS patterns of the polymers at 20°C and at 180°C; *h*00, 00l: Miller indices of reflections; dashed lines: scattering contributions of chains (h_{ch}); 003: peak from periodicity along backbones; h_π: peak from π-stacking of backbones; inset view: expansion of the (100) reflection q-range (PBTTT-^{8}O in blue and PBTTT-C_{12} in grey-black).

Table 1. Main macromolecular parameters of the synthesized PBTTTs.

	Mn (Da)	Đ	Td (°C)	HOMO level (eV)		ΔEg opt (eV)
				CV	PESA	
PBTTT-C_{12}	29600	1.82	386	-5.10	-4.80	1.9
PBTTT-^{8}O	30200	1.79	376	-4.95	-4.80	1.9

The polymer phase transitions of PBTTT-^{8}O and PBTTT-C_{12} were investigated using DSC, coupled with POM and SWAXS on powdered samples (Figures 1b, 1c and S7). For both polymers, the clearing transition to the isotropic phase is close to 200°C and very broad while the reverse transition upon cooling is observed with small delay, at similar temperatures (see Table S1 in the Supporting Information). In strong contrast to PBTTT-C_{12} that shows a clear transition between semi-crystalline and liquid crystalline phases around 139°C upon heating, no such phase transition is observed for PBTTT-^{8}O, for which the mesophase structure is frozen in glassy state at room temperature (Figures 1b and 1c). This means that *n*-C_7OC_4 side-chains do not crystallize, in strong contrast to the *n*-C_{12} side-chains of PBTTT-C_{12} that crystallize around 120°C, as shown by the transition in DSC and by the sharpening of the h_{ch} scattering signal in SWAXS pattern, and in agreement with previous literature data.[33,34] This lack of crystallinity observed for the PBTTT-^{8}O polymer and the corresponding bithiophene (**5**) can be explained by a hyperconjugation effect that tends to favor the synclinal conformation of the C-C bond next to the ether function. In contrast to

the anti-periplanar conformation usually observed in a pure linear alkyl chain, the synclinal conformation gives the side chain a bended shape that may prevent its crystallization (Figure S23).[35] As seen in the following, this important modification of the phase behavior of PBTTT-^{8}O has direct implications on the thermo-mechanical properties of the polymer that determine the alignment of the polymer using high-T rubbing. At ambient temperature, the SWAXS patterns of both powder polymers are characteristic of lamellar phases with interdigitated side-chains (Figure 1c). The good matching of molecular areas between thiophene monomer and side-chains drives the formation of stable lamellar structures that are maintained up to high temperature (180°C, see Table S2 in the Supporting Information) with strong interactions between π-stacked backbones combined to high correlation lengths (see Table S2 and Figure 1c). The smaller lamellar periodicity in PBTTT-^{8}O (d_{100}=18.95Å) is indicative of a more compact packing of the polymer substituted with *n*-C_7OC_4 than with *n*-C_{12} side-chains (d_{100}=20.46 Å).

The thermoelectric properties were subsequently measured for non-oriented thin-films of both polymers doped with F_6TCNNQ using the incremental concentration doping (ICD) protocol, previously introduced.[10] Most importantly, the doped thin films of PBTTT-^{8}O show quite superior charge conductivities as compared to PBTTT-C_{12} (see Table 2 and Figure S24). The conductivity in F_6TCNNQ-doped PBTTT-^{8}O can reach values of 1100 S/cm, close to values recently reported by Sirringhaus *et al*. on $FeCl_3$-doped PBTTT thin films,[36] *versus* 130±50 S/cm for PBTTT-C_{12}. The difference in charge conductivity between the two doped polymers can have two origins. Firstly, it may reflect a difference of charge carrier density related to a difference in the oxidation level between PBTTT-^{8}O and PBTTT-C_{12}. Indeed, a smaller ratio between the absorbances of the neutral polymer and the polaron P1 components in the UV-vis-NIR spectra of PBTTT-^{8}O (Figure 4b) supports a slightly higher apparent oxidation level for this polymer. Secondly, and more importantly, ED shows a different type of packing of PBTTT backbones in PBTTT-^{8}O with a much better defined order (multiple mixed index reflections are observed) that may well translate to larger charge mobilities in PBTTT-^{8}O. The larger charge conductivities in non-oriented films of PBTTT-

^{8}O do not translate to large thermoelectric PFs due to reduced Seebeck coefficients for PBTTT-^{8}O. The thermoelectric PF of both polymers are similar, in the range 25-30 $\mu W/m \cdot K^2$.

Table 2. Representative TE properties of non-oriented and oriented F_6TCNNQ-doped PBTTT-C_{12} and PBTTT-^{8}O thin-films.

	Non-rubbed films			Rubbed films			
	σ ($S.cm^{-1}$)	S ($\mu V.K^{-1}$)	PF ($\mu W.m^{-2}.K^{-1}$)		σ ($S.cm^{-1}$)	S ($\mu V.K^{-1}$)	PF ($\mu W.m^{-2}.K^{-1}$)
PBTTT-C_{12}	130±50	45±2	27±13	//	2430 ± 500	47 ± 7	530 ± 200
				⊥	200±100	15±2	3.5±0.5
PBTTT-^{8}O	1100±200	10±1	25±4	//	$5\pm2 \cdot 10^4$	24±2	2900±1600
				⊥	$1.3\pm0.2 \cdot 10^3$	4.3±0.5	2.4±0.9

2.2. Oriented thin films.

The higher charge conductivity obtained for the non-oriented doped PBTTT-^{8}O films was an incentive to probe the properties in aligned thin films. PBTTT thin films with very high anisotropy and solid-state order can be readily produced by using high-temperature rubbing.[37] The high polymer chain alignment translates to very high electrical conductivities and Seebeck coefficients in the chain direction after sequential doping with different type of dopants in orthogonal solvents such as acetonitrile.[27] The use of high temperatures upon rubbing is essential as it helps disentangle polymer chains when the side-chains are partially molten.[37] Moreover, for some polymers such as P3HT, rubbing close to the polymer melting temperature is a means to reach high crystallinity.[38] This is why different optimal rubbing temperature T_R could be expected for both PBTTT-^{8}O and PBTTT-C_{12}. Despite similar molar masses, both polymers exhibit different behavior upon high-T rubbing. Indeed, for PBTTT-C_{12} the optimized rubbing temperature (120°C) is limited by its transition towards the mesophase at $T_{C\text{-}LC}\approx$130°C and rubbing at T>125°C fully delaminates the films from the substrate. In strong contrast, the new single ether-based PBTTT-^{8}O can be aligned by rubbing up to 240°C. It presents an optimal alignment at T_R=170°C with a maximum

dichroic ratio of 20 (3D order parameter OP= 0.86) *versus* 10 (OP=0.75) at most for PBTTT-C_{12} rubbed at 120°C (Figure 2a). This result clearly underlines the beneficial effect of using a single ether group side-chain on the processing of PBTTT thin films by high-T rubbing. We attribute this effect to the stronger cohesive forces within layers of disordered and possibly entangled ether side-chains that cannot order to the same extent like the alkyl side-chains of PBTTT-C_{12}.

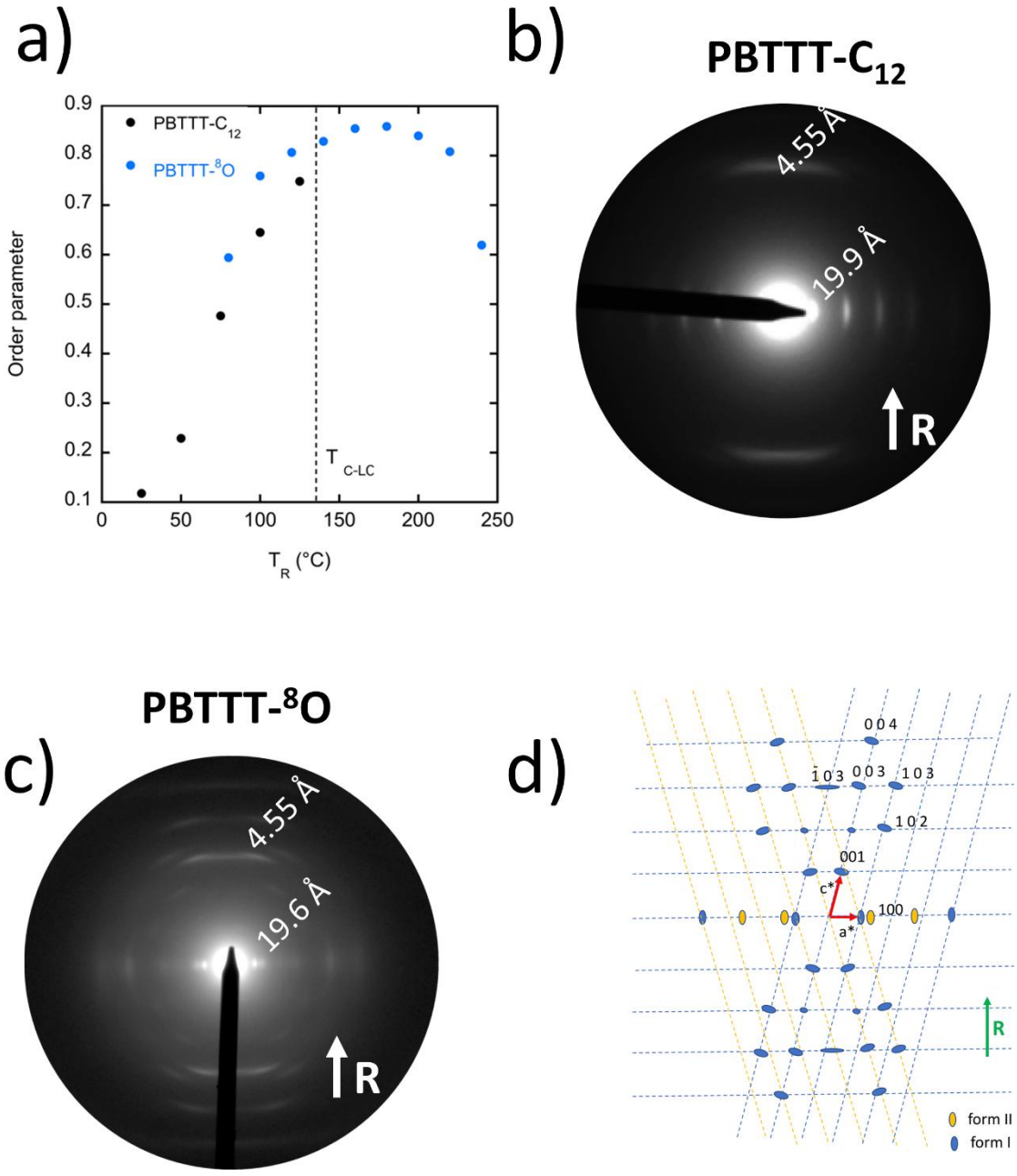

Figure 2. a) Evolution of the 3D order parameter versus rubbing temperature measured by polarized UV-vis-NIR spectroscopy in aligned PBTTT-^{8}O (red) and PBTTT-C_{12} (black) thin films. b) and c) Electron diffraction of thin films of PBTTT-C_{12} and PBTTT-^{8}O aligned by rubbing at 125°C and 170°C, respectively. R is the rubbing direction. d) Schematic illustration and indexation

of the ED pattern for PBTTT-^{8}O following a monoclinic unit cell.

Electron diffraction (Figures 2b and 2c) shows that despite having rather disordered *n*-C_7OC_4 side chains, the thin films of PBTTT-^{8}O aligned at 170°C show high structural order in the arrangement of the PBTTT backbones. The ED pattern of aligned PBTTT-^{8}O shows numerous mixed index reflections which are absent for PBTTT-C_{12}. The ED pattern of PBTTT-^{8}O films could be indexed considering a monoclinic unit cell with β =116° between the **a** and **c** axes (Figure 2d). This is a quite unusual and new structural signature for PBTTT induced by the ether-based side-chains. In strong contrast to PBTTT-^{8}O, the ED pattern of PBTTT-C_{12} in the lamellar C phase consists mainly of well-defined (*h* 0 0) (*h*=1-4) and some (0 0 l) reflections with *l*=3,4 without intense mixed index reflections. Close analysis of the ED of PBTTT-^{8}O gives also hints of polymorphism. A small fraction of a second polymorph (form II) is manifested by the presence of a second weak equatorial 1 0 0 reflection corresponding to a smaller lamellar periodicity d_{100}'=14.6-15.0 Å. Such polymorphism is not unexpected for PSCs and has been observed previously for other polymer such as regioregular poly(alkylthiophene)s.[39,40] It often reflects a difference in the tilt of the side chains to the backbone direction. In any case, this result shows that the introduction of a single oxygen atom in the alkyl side-chain modifies substantially the packing of PBTTT backbones as well as its phase behavior while maintaining structural order. Overall, these results are at strong variance with the findings of Thelakkat *et al*. as well as Nielsen *et al*. showing that the introduction of OEG side chains into poly(thiophene)s tends to disrupt the packing of backbones and reduces substantially structural order in the polymer.[25,26] The positive impact of a localized single ether group on the packing and ordering of PBTTT is thus clearly demonstrated.

The highly aligned PBTTT-^{8}O films were accordingly doped with F_6TCNNQ rather than $FeCl_3$ that helped reach conductivities beyond 10^5 S/cm for PBTTT-C_{12}. The benefits of using F_6TCNNQ over $FeCl_3$ are twofold: i) it is well intercalated in an ordered manner in the side chain layers of PBTTT-C_{12} and in addition ii) it leads to a greater stability of the doped PBTTT thin films (see anisotropic

TE properties section) as compared to $FeCl_3$ that de-dopes very rapidly.

Upon doping of oriented thin films of PBTTT-^{8}O and PBTTT-C_{12}, significant differences in the lattice variations with dopant concentration are evidenced (Figures 3a and S10). In general, sequential doping of PBTTT-C_{12} films results in a lattice expansion along the alkyl side-chains and a contraction along the π-stacking direction with a corresponding saturation at [F_6TCNNQ] = 2 g/l. For PBTTT-^{8}O the situation is remarkably different. First, a lattice expansion along the side-chain direction and a contraction in the π-stacking direction are seen already for a low dopant concentration (0.05 g/l, Figure S26 left). It is accompanied by the vanishing and smearing of some mixed index reflections, a fingerprint of dopant introduction in the crystal lattice of the polymer (see Figure S25).[9] However, very surprisingly, for [F_6TCNNQ] ≥ 0.5 g/l, the lattice dimensions tend to evolve back towards those of the undoped PBTTT-^{8}O phase, without recovering fully the initial values. Moreover, the diffraction pattern recovers sharp mixed index reflections. UV-vis-NIR spectroscopy shows that this behavior is not related to a de-doping of the thin films as the intensity of the polaronic bands P1 and P2 saturate for [F_6TCNNQ] ≥ 0.5 g/l (Figures 4a, 4b and S11). This original evolution of the lattice parameters suggests that a reorganization of the dopant molecules in the polymer matrix of PBTTT-^{8}O takes place at high doping levels.

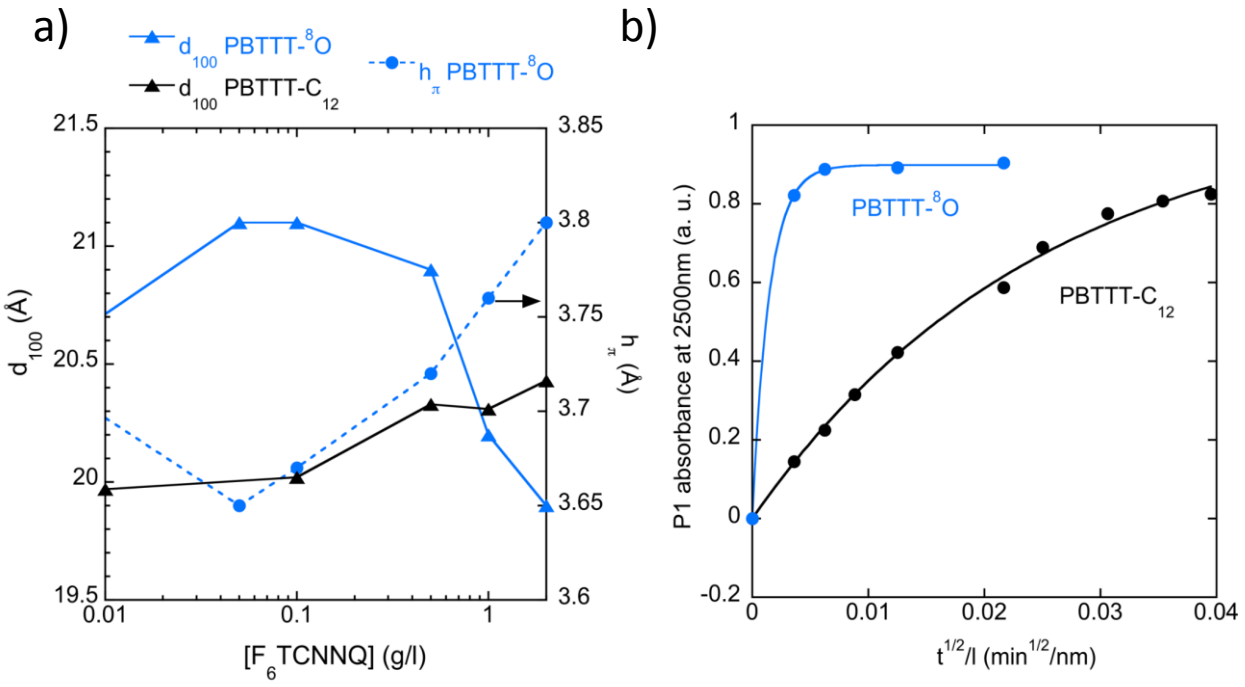

Figure 3. a) Evolution of the unit cell parameters d_{100} and h_π for oriented PBTTT-C_{12} and PBTTT-^{8}O thin films *versus* concentration of dopant [F_6TCNNQ] in acetonitrile. b) Comparison of the doping kinetics for PBTTT-C_{12} and PBTTT-^{8}O thin films with F_6TCNNQ as determined from the evolution of the absorbance of the polaron band P1 at 2500 nm ([F_6TCNNQ] = 1 g/l). The full lines are the results of the fits corresponding a diffusion-limited doping mechanism (see text).

Another particularity of PBTTT-^{8}O concerns the doping kinetics with F_6TCNNQ. It has been followed for both polymers by UV-vis-NIR spectroscopy on non-oriented thin films (Figure S28). The absorption intensities of the P1 and P2 bands, as a function of concentration and doping time, reflect the dopant diffusion into the polymer film and modeling the kinetics helps extract the dopant diffusion coefficients.[28] Using the approach proposed previously for PBTTT-C_{12},[41] we obtain diffusion coefficients of 7.8 10^{-11} cm^2/s *versus* 2.6 10^{-13} cm^2/s for PBTTT-^{8}O and PBTTT-C_{12}, respectively. In other words, F_6TCNNQ diffuses much faster into PBTTT-^{8}O than in PBTTT-C_{12}. Various hypotheses can be proposed to explain this result. Firstly, a higher affinity between the ether-based side-chains and the polar acetonitrile-based solution used to dope the thin films should be a driving force for faster dopant diffusion. Secondly, as mentioned in previous studies for

PBTTT thin films doped with F_4TCNQ, the crystallinity of the side chain limits the effective diffusion of the dopants.[28] TEM and DSC results indicate that ether-based side chains are quite disordered in PBTTT-^{8}O. A faster diffusion of the dopant is thus expected into the disordered side chains of PBTTT-^{8}O as compared to highly ordered and tightly packed C_{12} side chains.

2.3. Dopant distribution in side chain layers.

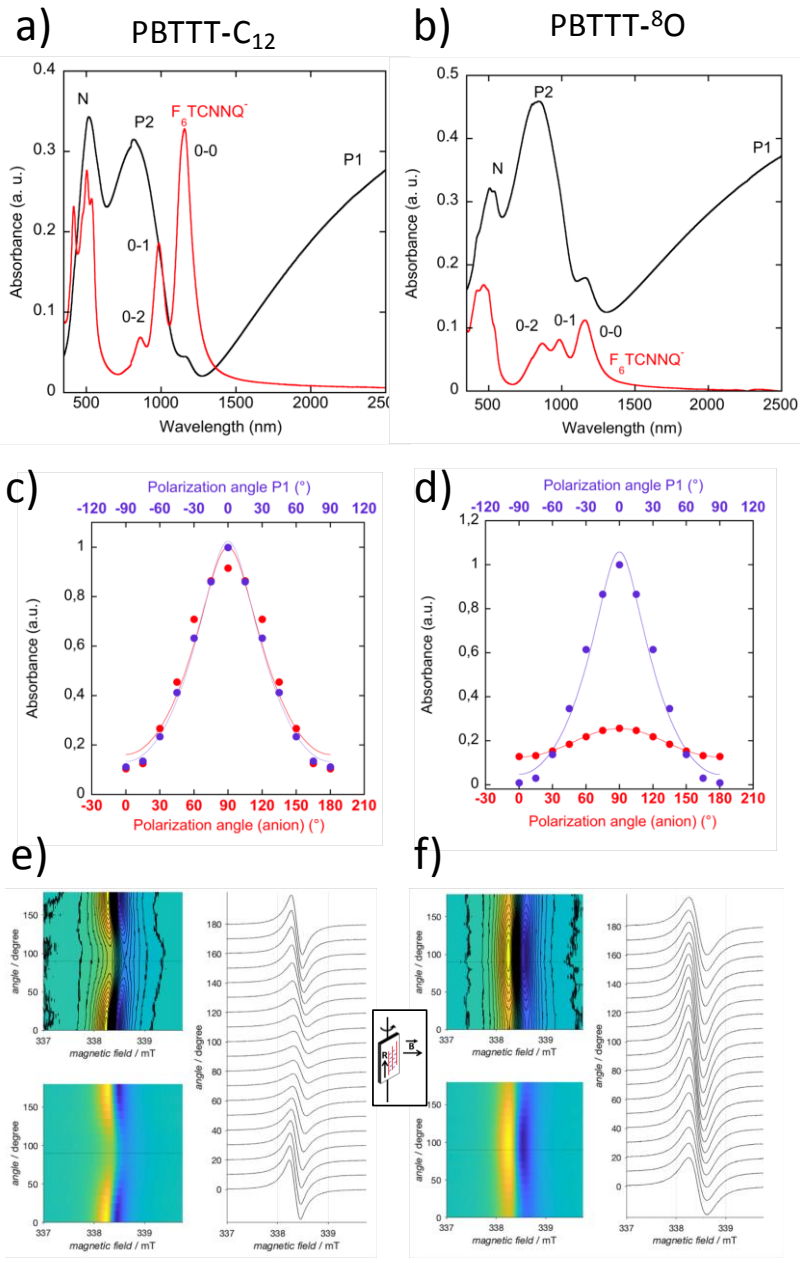

Figure 4. a) and b) Polarized UV-vis-NIR spectra of oriented thin films of PBTTT-C_{12} and PBTTT-^{8}O doped with F_6TCNNQ in acetonitrile (2 g/l). The light is polarized parallel (spectra in black) and perpendicular (spectra in red) to the rubbing. The main absorption polaronic bands (P1 and P2), neutral polymer (N) and of the F_6TCNNQ radical anion are highlighted. c) and d) Evolution of the absorbance of the P1 polaron band at 2500 nm (in violet) and of the F_6TCNNQ radical anion band at 1150 nm (in red) as a function of the polarization angle for both polymers. e) and f) EPR spectra obtained for both polymers as a function of the sample's rotation angle (see inset, 0° corresponds to the magnetic field in the film plane and 90° normal to the film plane).

Another evidence of the amorphous nature of PBTTT-^{8}O side-chains is manifested by the ordering of dopant molecules inside the polymer matrix. Angle-dependent polarized UV-vis-NIR absorption spectroscopy is an elegant method to probe the ordering of the dopant molecules within the polymer matrix. Indeed, both the P1 and P2 polaronic bands are polarized along the polymer backbone direction and $F_6TCNNQ^{\bullet-}$ absorption bands along the long axis of the dopant molecule (Figures 4a and 4b). Therefore, comparison of in-plane angular intensity distribution for both polaronic and dopant anion bands is a means to quantify their mutual orientation and ordering level. In oriented PBTTT-C_{12}, $F_4TCNQ^{\bullet-}$ and $F_6TCNNQ^{\bullet-}$ are intercalated in the layers of interdigitated side chains with their long axis oriented around a plane orthogonal to the average polymer chain direction.[10,28] Consequently, radical anion bands are polarized perpendicular to the rubbing direction. As shown in previous reports and in the figure 4c, in PBTTT-C_{12}, the maximum of angular distribution of $F_6TCNNQ^{\bullet-}$ bands is located at 90° to the PBTTT backbone direction (rubbing direction). Thus, the dopant molecules are distributed with their long axis in a plane orthogonal to the PBTTT-C_{12} backbone direction (Figure 5). The order parameter derived from the dichroic ratio for both the polaronic band (P1 at 2500 nm) and the dopant anion band (0-0 component at 1157 nm) shows that the ordering of $F_6TCNNQ^{\bullet-}$ in the PBTTT-C_{12} lattice is remarkable ($OP_{polaron}$=0.73 versus $OP_{F6TCNNQ\bullet-}$=0.70, Figure 4c). The situation is very different for F_6TCNNQ-doped PBTTT-^{8}O films.

First, despite similar intensities of polaronic bands, the absorbance of the $F_6TCNNQ^{\bullet-}$ radical anion band at 1157 nm is at least three times lower as compared to that found for PBTTT-C_{12} (despite slightly higher oxidation levels inferred from the intensity of polaronic bands, Figure 4b). Moreover, the in-plane angular distribution of the 0-0 anion band at 1157 nm is almost isotropic for PBTTT-^{8}O (Figure 4d). In PBTTT-^{8}O, the 3D order parameters for the polaronic and for the $F_6TCNNQ^{\bullet-}$ radical anion bands are 0.86 and 0.33, respectively (Figure 4d). This observation is accordingly fully consistent with the fact that the $F_6TCNNQ^{\bullet-}$ must be quite randomly oriented in the layers of *n*-C_7OC_4 side-chains as compared to the highly ordered and crystallized *n*-C_{12} side-chains of PBTTT-C_{12}. Further evidence for a rather disordered orientation distribution of $F_6TCNNQ^{\bullet-}$ in the matrix of PBTTT-^{8}O relates to the spectroscopic signature of the radical anion absorption. As seen in Figure 4b, the apparent absorbance of the 0-2 band of $F_6TCNNQ^{\bullet-}$ at 850 nm is substantially modified with the emergence of a new broad component overlapping it (for comparison, see the pure $F_6TCNNQ^{\bullet-}$ anion signature in solution in Figure S21 and doped PBTTT-C_{12} in Figure 4a). A similar occurrence of a new band overlapping the 0-2 band was previously reported for the cofacial dimers $(TCNQ^{\bullet-})_2$ in solution.[42] This spectral evolution is accordingly a fingerprint of $F_6TCNNQ^{\bullet-}$ clustering in the side-chain layers of PBTTT-^{8}O. This is in strong contrast with PBTTT-C_{12} for which a molecular dispersion of anions in the side chain layers without any evidence for dopant anion clustering is observed.

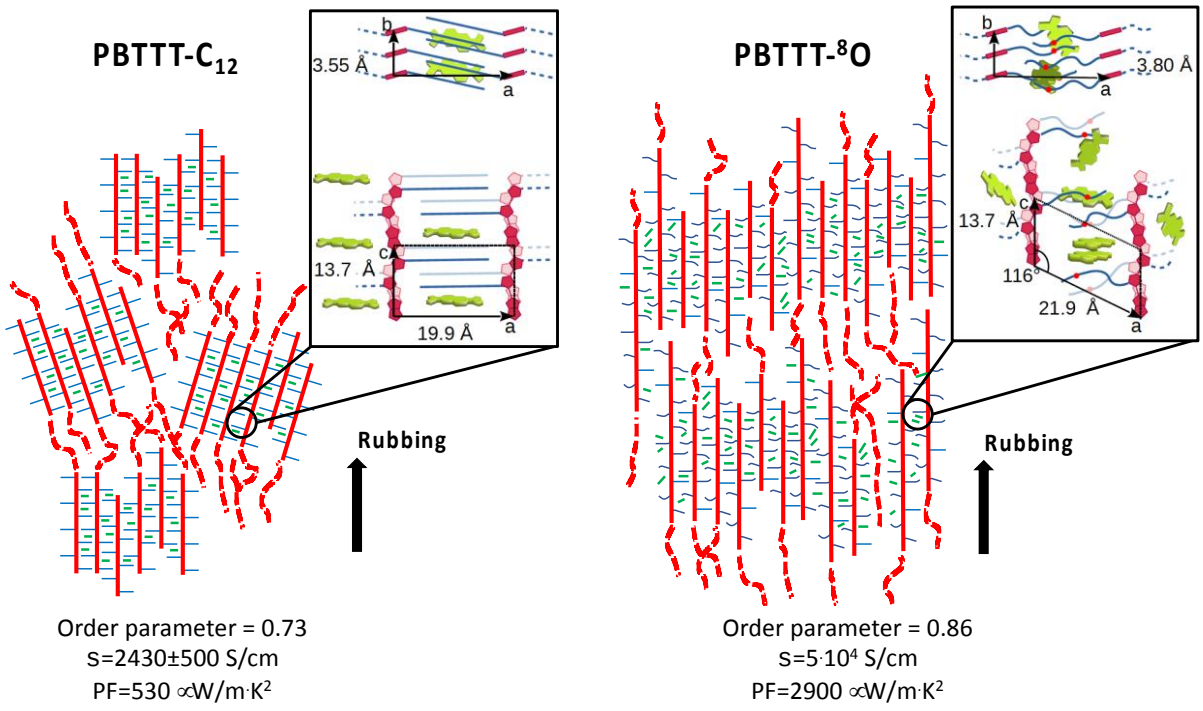

Figure 5. Schematic illustration of the meso-scale order induced by rubbing in PBTTT-C_{12} (left) and PBTTT-^{8}O (right), showing different organizations of the doped and aligned polymers, reached at 125°C for PBTTT-C_{12} versus 170°C in PBTTT-^{8}O. The $F_6TCNNQ^{\cdot -}$ dopant location and orientation within the layers of alkyl side chains of the two PBTTT polymers are represented in insets.

A final evidence for the disordered distribution of F_6TCNNQ radical anions in the side chain layers of PBTTT-^{8}O is obtained from electron paramagnetic resonance (EPR) measurements. In the solid state, spins interact with other spins via so-called dipolar interactions. These interactions are anisotropic in essence and must therefore reflect the local environment of the spins and the proximity of other spins. As shown for F_4TCNQ-doped P3HT films, the EPR signal features anisotropic characteristics depending on the orientation of polymer chains with respect to the magnetic field.[9] The anisotropy reflects differences in both orientations of the crystalline

polymeric domains on the substrate and orientation distribution of F_6TCNNQ radical anion in the polymer matrix. Since the films of both polymers show a dominant face-on orientation of domains, differences in the anisotropic EPR signal must reflect essentially differences in orientation distributions of the dopant radical anion inside the polymer films. When the sample is rotated around the rubbing direction (chain axis) in the magnetic field, a significant anisotropy of the EPR signal is observed for PBTTT-C_{12} in both shape and position (Figure 4e) whereas a similar rotation leaves the signal for doped PBTTT-^{8}O almost unaltered (Figure 4f). The observed EPR signal arises from the polaron on the polymer backbone and from the dopant radical anion. Turning the oriented film around the chain direction does not yield any anisotropy of the EPR signal from the polymer as the polymer chain remains perpendicular to the magnetic field. However, if the dopant molecules are oriented preferentially along the side chains in PBTTT-C_{12}, then a corresponding anisotropy of the EPR signal is expectedly evidenced when turning the sample around the polymer chain direction. In strong contrast, for dopant molecules randomly distributed inside the *n*-C_7OC_4 side chains of PBTTT-^{8}O, no anisotropy of the EPR signal is expected when turning the film around the polymer chain direction. Thus, the anisotropy of the EPR signals shown in Figures 4c and 4d can be fully ascribed to the ordering of the F_6TCNNQ dopant in the side-chain layers of PBTTT-C_{12} contrary to PBTTT-^{8}O for which dopants are more randomly oriented in the side-chain layers, fully consistent with the anisotropy of the optical data. Furthermore, the apparent larger line width of the EPR signal for PBTTT-^{8}O is consistent with the dopant clustering as deduced from the reduced absorption of the anion peak and the enhanced 0-2 band. Aggregation of dopant anions leads to enhanced dipolar interaction of adjacent F_6TCNNQ molecules reflected in an enhanced line width of the resulting EPR spectra.

2.4. Anisotropic TE properties.

Finally, TE properties were evaluated in rubbed thin films doped sequentially with F_6TCNNQ. As observed already for non-oriented films, the aligned PBTTT-^{8}O films reach very high conductivities

when doped with F_6TCNNQ. For PBTTT-^{8}O, the charge conductivity in the chain direction can reach up to $5 \cdot 10^4$ S/cm *versus* 2470 S/cm at maximum for PBTTT-C_{12} (see Figure S29a). The resulting PF increases from 0.53 mW/mK^2 for PBTTT-C_{12} to a maximum value of 2.9 mW/m$\cdot$K^2 for PBTTT-^{8}O (Table 1 and Figure S29c). Such a value is to the best of our knowledge the highest PF reported to date for doped *p*-type polymer semiconductors. It highlights the benefits of the introduction of a single ether group into the polymer side-chain (the electrical conductivity is already very high before rubbing, see Table 1) when combined with polymer alignment. It is worth to note that these values are comparable to the 2.10^5 S/cm and 2 mW/mK^2 previously obtained for aligned PBTTT-C_{12} doped with $FeCl_3$.[31] Importantly, as shown previously, the present combination PBTTT-^{8}O/F_6TCNNQ shows a much higher stability in time. Aligned PBTTT-^{8}O films doped with F_6TCNNQ retain a charge conductivity above 10^4 S/cm after 3 days in the glovebox whereas $FeCl_3$ doped films of PBTTT-C_{12} lose most of their conductivity within an hour (Figure S30).

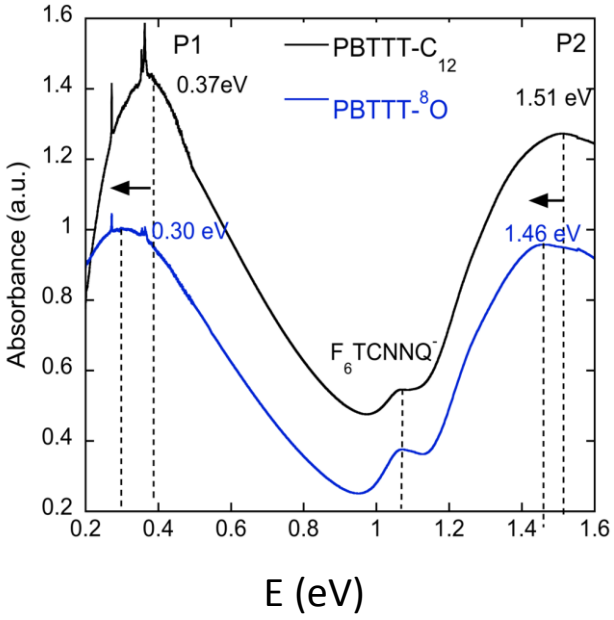

Figure 6. Vis-NIR-IR spectra of F_6TCNNQ-doped thin films of PBTTT-C_{12} (black) and PBTTT-^{8}O (blue).

The fact that the PBTTT-^{8}O polymer with poorest ordering of F_6TCNNQ dopants shows the highest

charge transport properties is surprising at a first glance. Recent investigations showed that ordering of dopant anions by intercalation in the pristine structure of poly(thiophenes) can lead to enhanced TE properties e.g. P3HT doped with F_4TCNQ and F_6TCNNQ.[43] The present results suggest that disordered side-chain layers and a disordered orientation distribution of dopant molecules is not necessarily detrimental for achieving high TE performances. It is known that polaron delocalization is one key parameter impacting the efficiency of doped PSCs. Recent works related the polaronic P1 peak position to its delocalization, which is dependent on the Coulombic charge interactions occurring between polarons and radical anions. As a consequence, it has been shown that the energy position of the P1 band is determined, at least in part, by the distance between the PSC backbone and the dopant radical anion. The position of the P1 band is thus a marker of the polaron delocalization.[44,45] By moving the radical anion away from the conjugated backbone, one expects to observe a higher delocalization of the polaron i.e. a red shift of the P1 peak. A combination of UV-vis-NIR and FTIR spectroscopies was used to analyze the lower-energy P1 sub-gap transition in both polymers upon doping (Figure 6). PBTTT-^{8}O exhibits a P1 peak red-shifted of about 0.07 eV as regards to PBTTT-C_{12}. Thus, the radical anion can be assumed to be on average a little further away from the positive polaron formed on the PBTTT conjugated backbone. This can be explained by the rather disordered orientation distribution of $F_6TCNNQ^{\bullet -}$ dopants, evidenced in this study. Indeed, in rubbed PBTTT-C_{12}, orienting the $F_6TCNNQ^{\bullet -}$ molecules strictly perpendicular to the PBTTT backbone brings the negatively charged cyano groups of the dopant radical anion in close proximity to the polaronic charges on the backbones, limiting the polaron delocalization. In strong contrast, when the $F_6TCNNQ^{\bullet -}$ are more randomly oriented in the side chain layers, the partial negative charges carried by the cyano groups will be on average further away from the conjugated backbone, in particular if we assume that the dopants interact weakly with the ether groups, located on average in the middle of the side-chain layer (see schematic illustration on Figure 5). Consequently, the coulombic interactions between polarons and radical anions should be decreased, favoring polaron delocalization. It is also worth mentioning that the dielectric constant of

polymers bearing oligo(ethyleneglycol) side chains can be substantially increased as compared to the analogue polymers with alkyl side chains, giving thus a further origin for screening of Coulomb interactions between the dopant anion and the polaron.[46] Other aspects such as the level of in-plane orientation of the PBTTT backbones may be equally important to observe high charge conductivities. Clearly the OP defining in-plane orientation of PBTTT chains is significantly improved for PBTTT-^{8}O (OP=0.86) thanks to the use of a higher rubbing temperature. Recent theoretical investigation by Ihnatsenka shows that the charge conductivity anisotropy $\sigma_{//}/\sigma_{\perp}$ should increase exponentially with the degree of chain orientation.[47]

3. Conclusion.

While the introduction of OEG side-chains can be beneficial to enhance TE properties of doped polymer semiconductors e.g. by coprocessing of polymer and dopant in a common solvent, it can also adversely affect structure and stability of the systems due to the air-sensitive character of OEG-side-chain based polymer as well as the fact that it can substantially modify ordering of the polymers.[25] In this work, we demonstrate that the introduction of a single ether group in the linear alkyl side-chains is an effective strategy to enhance substantially the TE performances of oriented F_6TCNNQ-doped PBTTTs. Such a side-chain modification preserves the structural order of PBTTT and improves thermomechanical properties of the thin films that can be oriented to reach very high dichroic ratios up to 20 at temperatures of 170°C thanks to enhanced cohesive forces within side-chain layers. A combination of polarized UV-vis-NIR and EPR spectroscopies showed that F_6TCNNQ radical anions are rather disordered in the side chain layers of PBTTT-^{8}O, including some dopant clusters, contrary to PBTTT-C_{12}. The disordered distribution of dopant radical anions in PBTTT-^{8}O is presently attributed to the combination of disordered side-chains and weak dipolar interactions between the side-chain ether groups and the dopant which result in an overall increase of the dopant-polaron distance. As a consequence, PBTTT-^{8}O films rubbed at 170°C exhibit an improved conductivity by more than one order of magnitude as compared to PBTTT-C_{12}.

Enhancement of both charge conductivity and Seebeck coefficient in the chain direction of PBTTT-^{8}O results in very high and record thermoelectric PF of up to 2.9 mW/mK^{2}. Tailoring single ether side-chains in polymer semiconductors could also be beneficial for a larger palette of applications. For instance, organic electrochemical transistors (OECTs) require a high diffusivity of dopants within the polymer film together with a suitable charge transport property, essential to achieve fast switching of the devices.[23,48] Thus, this new ether-based side chain functionalization allowing to combine high conjugated polymer backbone order and ion diffusivity, is a promising macromolecular engineering strategy. Fine tuning of the ether position within the side-chain is a further degree of freedom that will be investigated in a forthcoming publication.

Acknowledgements: The authors gratefully acknowledge Dr. Fanny Richard and Pr. Paolo Samori (ISIS, Strasbourg) for carrying out PESA measurements and Dr. Olivier Boyron for the SEC measurements**.** We thank the Agence Nationale de la Recherche for financial support through project ANR-17-CE05-0012 (ANISOTHERM), region Grand'Est for the co-funding of Pablo Durand and CNRS through PEPS grant Thermobody.

References

[1] H. Bronstein, C. B. Nielsen, B. C. Schroeder, I. McCulloch, *Nat. Rev. Chem.* **2020**, *4*, 66.

[2] Z.-Q. Jiang, C. Poriel, N. Leclerc, *Mater. Chem. Front.*, **2020**, *4*, 2497.

[3] W. Zhao, J. Ding, Y. Zou, C.-A. Di, D. Zhu, *Chem. Soc. Rev*., **2020**, *49*,7210.

[4] M. Lindorf, K. A. Mazzio, J. Pflaum, K. Nielsch, W. Brütting, M. Albrecht, *J. Mater. Chem. A*, **2020**, 8,7495.

[5] O. Bubnova, X. Crispin, *Energy Environ. Sci*. **2012**, *5*, 9345.

[6] A. M. Glaudell, J. E. Cochran, S. N. Patel, M. L. Chabinyc, *Adv. Energy Mater*. **2015**, *5*, 1401072.

[7] D. Kiefer, R. Kroon, A. I. Hofmann, H. Sun, X. Liu, A. Giovannitti, D. Stegerer, A. Cano, J.

Hynynen, L. Yu, Y. Zhang, D. Nai, T. F. Harrelson, M. Sommer, A. J. Moulé, M. Kemerink, S. R. Marder, I. McCulloch, M. Fahlman, S. Fabiano, C. Müller, *Nature Mater*. **2019**, *18*, 149.

[8] E. Lim, K. A. Peterson, G. M. Su and M. L. Chabinyc, *Chem. Mater*. **2018**, *30*, 998.

[9] V. Untilova, T. Biskup, L. Biniek, V. Vijayakumar, M. Brinkmann, *Macromolecules* **2020**, *53*, 2441.

[10] V. Vijayakumar, P. Durand, H. Zeng, V. Untilova, L. Herrmann, P. Algayer, N. Leclerc, M. Brinkmann, *J. Mater. Chem. C* **2020**, *8*, 16470.

[11] J. Mei, Z. Bao, *Chem. Mater*. **2014**, *26*, 1, 604.

[12] A. Giovannitti, I. P. Maria, D. Hanifi, M. J. Donahue, D. Bryant, K. J. Barth, B. E. Makdah, A. Savva, D. Moia, M. Zetek, P. R. F. Barnes, O. G. Reid, S. Inal, G. Rumbles, G. G. Malliaras, J. Nelson, J. Rivnay, I. McCulloch, *Chem. Mater*. **2018**, *30*, 2945.

[13] B. Meng, H. Song, X. Chen, Z. Xie, J. Liu, L. Wang, *Macromolecules* **2015**, *48*, 4357.

[14] J. Liu, L. Qiu, G. Portale, M. Koopmans, G. Ten Brink, J. C. Hummelen, L. J. A. Koster, *Adv. Mater*. **2017**, *29*, 1701641

[15] J. Li, C. W. Rochester, I. E. Jacobs, E. W. Aasen, S. Friedrich, P. Stroeve, A. J. Moulé, *Org. Electron*. **2016**, *33*, 23.

[16] R. Kroon, D. Kiefer, D. Stegerer, L. Yu, M. Sommer, C. Müller, *Adv. Mater*. **2017**, *29*, 1700930.

[17] A. I. Hofmann, R. Kroon, L. Yu, C. Müller, *J. Mater. Chem. C* **2018**, *6*, 6905.

[18] A. Giovannitti, D.-T. Sbircea, S. Inal, C. B. Nielsen, E. Bandiello, D. A. Hanifi, M. Sessolo, G. G. Malliaras, I. McCulloch, J. Rivnay, *Proc. Natl. Acad. Sci. USA* **2016**, *113*, 12017.

[19] D. Kiefer, A. Giovannitti, H. Sun, T. Biskup, A. Hofmann, M. Koopmans, C. Cendra, S. Weber, L. J. Anton Koster, E. Olsson, J. Rivnay, S. Fabiano, I. McCulloch, C. Müller, *ACS Energy Lett*. **2018**, *3*, 278.

[20] Y.-H. Shin, H. Komber, D. Caiola, M. Cassinelli, H. Sun, D. Stegerer, M. Schreiter, K. Horatz, F. Lissel, X. Jiao, C. R. McNeill, S. Cimo, C. Bertarelli, S. Fabiano, M. Caironi, M. Sommer,

Macromolecules **2020**, *53*, 5158.

[21] N. Leclerc, A. Michaud, K. Sirois, J.-F. Morin, M. Leclerc, *Adv. Func. Mater*. **2006**, *16*, 1694.

[22] B. X. Dong, C. Nowak, J. W. Onorato, T. Ma, J. Niklas, O. G. Poluektov, G. Grocke, M. F. DiTusa, F. A. Escobedo, C. K. Luscombe, P. F. Nealey, S. N. Patel, *Chem. Mater*. **2021**, *33*, 741.

[23] R. K. Hallani, B. D. Paulsen, A. J. Petty II, R. Sheelamanthula, M. Moser, K. J. Thorley, W. Sohn, R. B. Rashid, A. Savva, S. Moro, J. P. Parker, O. Drury, M. Alsufyani, M. Neophytou, J. Kosco, S. Inal, G. Costantini, J. Rivnay, I. McCulloch, *J. Am. Chem. Soc*. **2021**, *143*, 11007.

[24] T. Ma, B. X. Dong, G. L. Grocke, J. Strzalka, S. N. Patel, *Macromolecules* **2020**, *53*, 2882.

[25] P. Schmode, A. Savva, R. Kahl, D. Ohayon, F. Meichsner, O. Dolynchuk, T. Thurn-Albrecht, S. Inal, M. Thelakkat, *ACS Appl. Mater. Interfaces* **2020**, *12*, 13029.

[26] P. A. Finn, I. E. Jacobs, J. Armitage, R. Wu, B. D. Paulsen, M. Freeley, M. Palma, J. Rivnay, H. Sirringhaus, C. B. Nielsen, *J. Mater. Chem. C* **2020**, *8*, 16216.

[27] A. Hamidi-sakr, L. Biniek, J.-L. Bantignies, D. Maurin, L. Herrmann, N. Leclerc, P. Lévêque, V. Vijayakumar, N. Zimmermann, M. Brinkmann, *Adv. Funct. Mater*. **2017**, *27*, 1700173.

[28] V. Vijayakumar, E. Zaborova, L. Biniek, H. Zeng, L. Herrmann, A. Carvalho, O. Boyron, N. Leclerc, M. Brinkmann, *ACS Appl. Mater. Interfaces* **2019**, *11*, 4942.

[29] D. T. Scholes, S. A. Hawks, P. Y. Yee, H. Wu, J. R. Lindemuth, S. H. Tolbert, B. J. Schwartz, *J. Phys. Chem. Lett*., **2015**, *6*, 4786.

[30] I. E. Jacobs, E. W. Aasen, J. L. Oliveira, T. N. Fonseca, J. D. Roehling, J. Li, G. Zhang, M. P. Augustine, M. Mascal, A. J. Moulé *J. Mater. Chem. C*, **2016**, *4*, 3454.

[31] V. Vijayakumar, Y. Zhong, V. Untilova, M. Bahri, L. Herrmann, L. Biniek, N. Leclerc, M. Brinkmann, *Adv. Energy Mater*. **2019**, *9*, 1900266.

[32] J. W. Onorato, Z. Wang, Y. Sun, C. Nowak, L. Q. Flagg, R. Li, B. X. Dong, L. J. Richter, F. A. Escobedo, P. F. Nealey, S. N. Patel, C. K. Luscombe, *J. Mater. Chem. A* **2021**,*9*, 21410.

[33] I. McCulloch, M. Heeney, C. Bailey, K. Genevicius, I. MacDonald, M. Shkunov, D. Sparrowe, S. Tierney, R. Wagner, W. Zhang, M. L. Chabinyc, R. J. Kline, M. D. McGehee, M. F. Toney, *Nat.*

Mater. **2006**, 5, 328.

[34] D. M. DeLongchamp, R. J. Kline, Y. Jung, E. K. Lin, D. A. Fischer, D. J. Gundlach, S. K. Cotts, A. J. Moad, L. J. Richter, M. F. Toney, M. Heeney, I. McCulloch, *Macromolecules*, **2008**, *41*, 5709.

[35] I. V. Alabugin, G. dos Passos Gomes, M. A. Abdo, *WIREs Comput Mol Sci*. **2019**, e1389.

[36] I. E. Jacobs, Y. Lin, Y. Huang, X. Ren, D. Simatos, C. Chen, D. Tjhe, M. Statz, L. Lai, P. A. Finn, W. G. Neal, G. D'Avino, V. Lemaur, S. Fratini, D. Beljonne, J. Strzalka, C. B. Nielsen, S. Barlow, S. R. Marder, I. McCulloch, H. Sirringhaus, *Adv. Mater*. **2021**, doi.org/10.1002/adma.202102988.

[37] L. Biniek, S. Pouget, D. Djurado, E. Gonthier, K. Tremel, N Kayunkid, E. Zaborova, N. Crespo-Monteiro, O. Boyron, N. Leclerc, S. Ludwigs, M. Brinkmann, *Macromolecules*, **2014**, *47*, 3871.

[38] A. Hamidi-Sakr, D. Schiefer, S. Covindarassou, L. Biniek, M. Sommer, M. Brinkmann, *Macromolecules*, **2016**, *49*, 3452.

[39] T. J. Prosa, M. J Winokur, R. D. McCullough, *Macromolecules*, **1996**, *29*, 3654.

[40] M. Brinkmann, *J. Polym. Sci., Part B: Polym. Phys.* **2011**, *49*, 1218.

[41] J. Li, C. Koshnick, S. O. Diallo, S. Ackling, D. M. Huang, I. E. Jacobs, T. F. Harrelson, K. Hong, G. Zhang, J. Beckett, M. Mascal, A. J. Moulé, *Macromolecules* **2017**, *50*, 5476.

[42] R. H. Boyd, W. D. J. Phillips, *Chem. Phys.* **1965**, *43*, 2927.

[43] V. Untilova, H. Zeng, P. Durand, L. Herrmann, N. Leclerc, M. Brinkmann, *Macromolecules*, **2021**, *54*, 6073.

[44] T. J. Aubry, J. C. Axtell, V. M. Basile, K. J. Winchell, J. R. Lindemuth, T. M. Porter, J. Y. Liu, A. N. Alexandrova, C. P. Kubiak, S. H. Tolbert, A. M. Spokoyny, B. J. Schwartz, *Adv. Mater*. **2019**, *31*, 1805647.

[45] R. Ghosh, A. R. Chew, J. Onorato, V. Pakhnyuk, C. K. Luscombe, A. Salleo, F. C. Spano, *J. Phys. Chem. C* **2018**, *122*, 18048.

[46] J. Brebels, E. Douvogianni, D. Devisscher, R. Thiruvallur Eachambadi, J. Manca, L. Lutsen, D. Vanderzande, J. C. Hummelen, W. J. Maes, *Mater. Chem. C* **2018**, *6*, 500.

[47] S. Ihnatsenka, arXiv:2108.06097 [cond-mat.mes-hall].

[48] B. D. Paulsen, K. Tybrandt, E. Stavrinidou, J. Rivnay, *Nature Mater*. **2020**, *19*, 13.

Table of Content

The use of an ether-based side chain leads to a new class of slightly polar PBTTT polymers. This side-chain preserves the ease of synthesis and the air stability while improving the structural order of conjugated backbones and thermomechanical properties. After rubbing and F_6TCNNQ-doping, very high charge conductivity $\sigma = 5 \cdot 10^4$ S/cm and a record power factor PF = 2.9 $mWm^{-1}K^{-2}$ were obtained.